ACS Energy LETTERS

Cite This: ACS Energy Lett. 2019, 4, 2368−2377

http://pubs.acs.org/journal/aelccp

# $V^{2+}/V^{3+}$ Redox Kinetics on Glassy Carbon in Acidic Electrolytes for Vanadium Redox Flow Batteries

Harsh Agarwal, Jacob Florian, Bryan R. Goldsmith, and Nirala Singh*

Department of Chemical Engineering, University of Michigan, Ann Arbor, Michigan 48109-2136, United States

Catalysis Science and Technology Institute, University of Michigan, Ann Arbor, Michigan 48109-2136, United States

Supporting Information

**ABSTRACT:** Vanadium redox flow batteries are a promising technology for energy storage, yet the mechanism of the kinetically limiting $V^{2+}/V^{3+}$ redox reaction remains poorly understood. Here, we elucidate the impact of anion complexation on $V^{2+}/V^{3+}$ kinetics on a glassy carbon electrode in three common electrolytes: hydrochloric acid, sulfuric acid, and mixed $HCl/H_2SO_4$. The $V^{2+}/V^{3+}$ kinetics are ∼2.5 times faster in HCl and have lower apparent activation energies than those in $H_2SO_4$ or $HCl/H_2SO_4$. We also identify the presence of $[V(H_2O)_4Cl_2]^+$ species in HCl by UV−vis spectroscopy. We confirm that the $V^{2+}/V^{3+}$ reaction proceeds via an adsorbed intermediate and propose a bridging mechanism through adsorbed *Cl (in HCl) and *OH (in $H_2SO_4$ or $HCl/H_2SO_4$). A bridging mechanism through *Cl is supported by even faster redox kinetics in HBr than in HCl, possibly due to the higher polarizability of *Br. By measuring the exchange current densities using steady-state current measurements and impedance spectroscopy, we show that the overall reaction is a two-electron process in HCl as opposed to a one-electron process in $H_2SO_4$ and $HCl/H_2SO_4$.

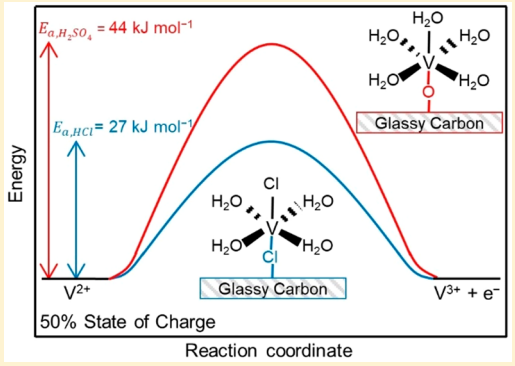


Electricity demand continues to increase because of the world's rising population and standard of living. This increasing demand is currently met by burning fossil fuels, which adversely impacts the global climate through rising $CO_2$ emissions (∼16% increase in the past decade and estimated to reach 39 billion tons per year by 2040).[1] A sustainable way to meet our world's electricity needs is to use renewable electricity sources like solar and wind, but their intermittent nature necessitates storing this electricity and releasing based on demand. Although pumped hydroelectricity currently provides the majority of electricity storage, its geographical limitations have led to searches for alternative electricity storage technologies.[2,3]

Redox flow batteries (RFBs), since their inception in 1974 by Thaller,[4] have shown tremendous capability to store and release renewable electricity at a multimegawatt-hours scale.[3] Advantages of RFBs over stationary electrode batteries include decoupled power and energy due to the RFB's external storage of the electrolyte and long lifetimes (>10 000 cycles,[3] > 20 years) because RFB electrodes act as electrocatalysts rather than participate directly in the redox reaction.[5] These attributes provide RFBs high flexibility and scalability for grid energy storage applications.[6,7]

Aqueous RFBs involving solely vanadium ions[8] (VRFBs: $VO_{2+}/VO^{2+}//V^{2+}/V^{3+}$) are among the most well-developed aqueous RFBs, attracting investments close to a billion dollars in recent years for large-scale energy storage deployment,[9] with 209.8 MWh of energy capacity installed as of 2019.[10] Using only vanadium ions in both half-cells of VRFBs eliminates the challenge of cross-contamination,[11] which is responsible for permanent capacity losses in other aqueous RFB systems. Nevertheless, VRFBs suffer from a high activation (kinetic) overvoltage of the slower $V^{2+}/V^{3+}$ redox couple ($V^{2+} \rightleftarrows V^{3+} + e^-$, $E^\circ = -0.255$ V vs SHE) that lowers overall round-trip energy storage efficiency.[11] In existing systems, eliminating the $V^{2+}/V^{3+}$ redox couple overvoltage[12,13] by improving the $V^{2+}/V^{3+}$ redox kinetics could increase this efficiency from 77 to ∼86%.[14] In addition, faster redox kinetics would enable switching to thinner, lower surface area carbon papers from thicker, high surface area porous carbon felts, which would lower the overall ohmic resistance of the battery.[15]

Despite VRFBs being the most well-developed RFB and closest to commercial implementation for large-scale energy storage, there is a lack of fundamental understanding of $V^{2+}/V^{3+}$ redox couple chemistry, particularly the role of electrolyte

Received: July 3, 2019
Accepted: September 3, 2019
Published: September 3, 2019





DOI: 10.1021/acsenergylett.9b01423
ACS Energy Lett. 2019, 4, 2368−2377

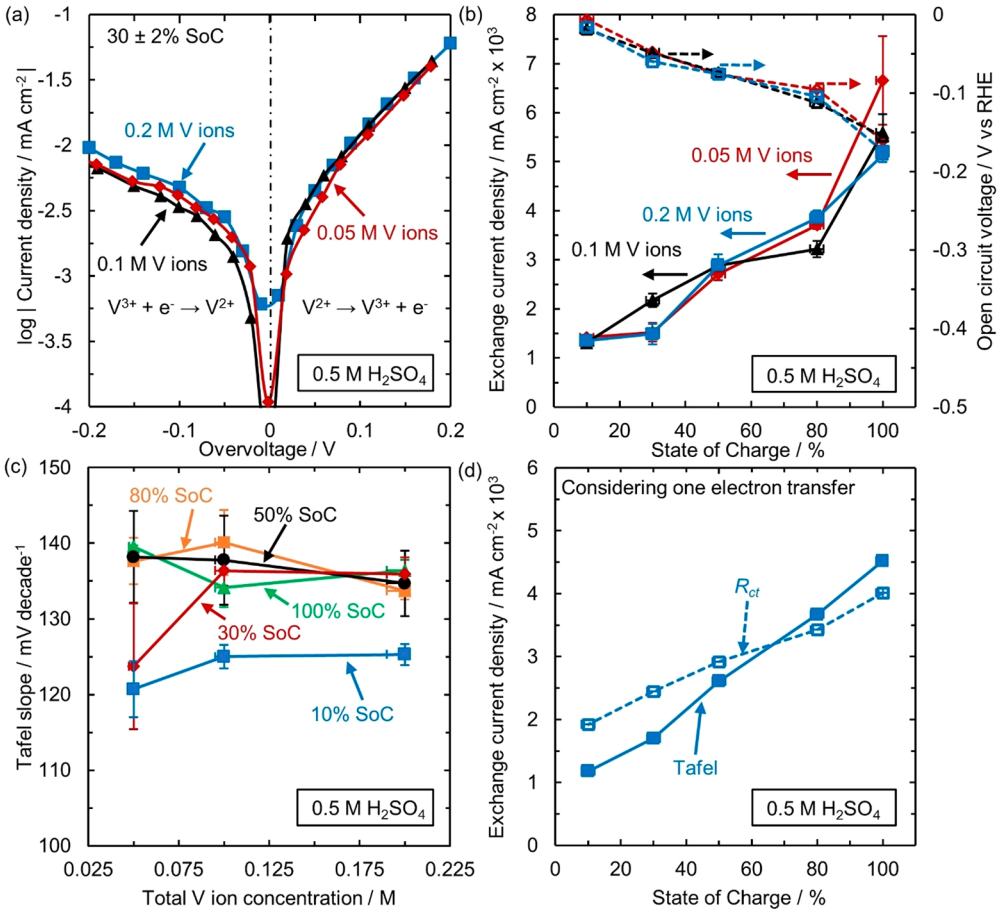


**Figure 1. $V^{2+}/V^{3+}$ kinetics in $H_2SO_4$ at room temperature ($T$ = 23.3 °C). (a) Log of the absolute value of current densities vs overvoltage at 30% SoC for 0.05, 0.1, and 0.2 M total vanadium concentrations. (b) Exchange current densities obtained by using the Tafel equation plotted as a function of SoC for 0.05, 0.1, and 0.2 M total vanadium. The OCVs vs RHE as a function of SoC are also shown. (c) Tafel slope as a function of SoC for 0.05, 0.1, and 0.2 M total vanadium. (d) Exchange current densities as a function of SoC for 0.2 M total vanadium by two independent methods: (i) (solid line) Using the Tafel equation as in (b) and (ii) (dashed line) charge transfer resistance at OCV using potentiostatic electrochemical impedance measurements assuming a total of one-electron transfer. The total $SO_4^{2-}$ concentration is changing with total vanadium concentration due to the use of $VOSO_4$ as the precursor salt. The supporting electrolyte is 0.5 M $H_2SO_4$, and a glassy carbon working electrode disk rotating at $\omega$ = 1500 rpm is used to remain in the kinetic regime.**

on the redox couple and the associated charge transfer. VRFBs with carbon electrodes employing HCl[16−18] or mixed acid electrolytes (i.e., $HCl/H_2SO_4$)[19−21] have higher current densities and greater vanadium ion stability compared with the traditionally used $H_2SO_4$ electrolyte. Nevertheless, the structure of the vanadium ion complexes in these electrolytes is not well understood, and it is unclear if the improved current densities are related to kinetics (as opposed to mass transport or conductivity). The $V^{2+}$ and $V^{3+}$ ions in pure water or in noncomplexing electrolytes such as perchloric acid exist as $[V(H_2O)_6]^{2+}$ and $[V(H_2O)_6]^{3+}$, respectively, with each of the six water molecules located at the ends of an octahedron ($O_h$ symmetry), constituting the first coordination sphere around the vanadium ion.[22,23] In certain acidic electrolytes (e.g., HCl, $H_2SO_4$, and $H_3PO_4$), anions can replace water molecules in the first coordination sphere of $V^{2+}$ and $V^{3+}$, as shown in previous studies.[24−28] Because the choice of electrocatalyst has been shown qualitatively to impact the $V^{2+}/V^{3+}$ kinetics,[29−34] the $V^{2+}/V^{3+}$ reaction has been postulated to involve inner-sphere electron transfer. However, further quantitative work is needed to confirm whether the electron transfer is inner- or outer-sphere and to understand the structure of the vanadium complexes in acidic electrolytes used in VRFBs. Here we show new evidence that the $V^{2+}/V^{3+}$ reaction is inner-sphere electron transfer and link the kinetics of the $V^{2+}/V^{3+}$ reaction on a carbon electrode with the vanadium complex structure in three commonly used electrolytes—hydrochloric acid, sulfuric acid, and mixed $HCl/H_2SO_4$.

In this study, we identify the $V^{2+}$ and $V^{3+}$ complexes using UV−vis and examine $V^{2+}/V^{3+}$ redox kinetics on a glassy carbon electrode. The $V^{2+}/V^{3+}$ redox kinetics are enhanced in HCl compared with $H_2SO_4$ or $HCl/H_2SO_4$ mixtures, based on our higher measured exchange current densities ($i_o$) and lower apparent activation energies ($E_a$) from both steady-state current measurements and impedance spectroscopy. These rates and activation energies depend on the $V^{2+}$ and $V^{3+}$ concentrations, with a negative order in $V^{3+}$ that supports the hypothesis of an inner-sphere, adsorption-mediated step in all electrolytes. From experimental UV−vis studies, we confirm that $V^{2+}$ exists as $[V(H_2O)_6]^{2+}$ in all electrolytes, with no anions in the first coordination shell. Our experimental and computational UV−vis measurements show that $V^{3+}$ exists as a distribution of complexes, with a majority of water/sulfate-complexed species, $[V(H_2O)_5SO_4]^{+}$, and a minority of water-complexed species, $[V(H_2O)_6]^{3+}$, in both $H_2SO_4$ and $HCl/H_2SO_4$. In HCl, $V^{3+}$ exists as a majority of water-complexed



DOI: 10.1021/acsenergylett.9b01423
ACS Energy Lett. 2019, 4, 2368−2377

species, $[V(H_2O)_6]^{3+}$, and a minority of water/chloride-complexed species, $[V(H_2O)_4Cl_2]^{+}$. We propose that the enhanced $V^{2+}/V^{3+}$ kinetics in HCl compared with those in $H_2SO_4$ and $HCl/H_2SO_4$ are due to the charge transfer proceeding through chloride bridges (*Cl) on the glassy carbon surface in HCl, instead of through surface-bound hydroxyl (*OH) groups[35,36] in $H_2SO_4$ and $HCl/H_2SO_4$. This hypothesis of electron transfer through bridges is supported by the faster $V^{2+}/V^{3+}$ redox kinetics that we measure in HBr compared with those in HCl. This enhancement is expected for a bridging mechanism due to the greater deformability of the bromide (*Br) bridges than *Cl bridges,[37] which accelerates the electron transfer between the adsorbed species and the electrode through the bridge.

The redox kinetics of $V^{2+}/V^{3+}$ are examined in three electrolytes, "HCl" (0.2 M $VCl_3$ + 1 M HCl), "$H_2SO_4$" (0.2 M $VOSO_4$ + 0.5 M $H_2SO_4$) and "$HCl/H_2SO_4$" (0.2 M $VCl_3$ + 0.5 M $H_2SO_4$), to analyze how different anions ($Cl^-$ and $SO_4^{2-}$) impact the kinetics of the $V^{2+}/V^{3+}$ redox couple on a glassy carbon surface. Either $VCl_3$ or $VOSO_4$ is used to avoid the presence of any sulfate or chloride anions in the HCl and $H_2SO_4$ electrolyte, respectively. We also study the kinetics in HBr to test the bridging mechanism hypothesis proposed in this work. Electrolytes in noncomplexing perchloric acid ($HClO_4$) are prepared to serve as standards for UV−vis measurements. Section S1 of the Supporting Information (SI) discusses the details of preparing these electrolytes. The state of charge $\left(\mathrm{SoC} = \frac{[V^{2+}]}{[V^{2+}] + [V^{3+}]}\right)$ is controlled by electrochemically oxidizing or reducing the working electrolyte. $V^{2+}$ and $V^{3+}$ concentrations are confirmed using UV−vis spectroscopy by fitting Gaussian peaks to calibration standards (section S1). Fitted UV−vis spectra of $V^{2+}$ and $V^{3+}$ are shown in Figures S1 and S2 with calibration parameters in Tables S1 and S2. Time-dependent density functional theory (TDDFT) is used to predict UV−vis spectra of different $V^{3+}$ complexes (all TDDFT methodology details are available in section S2). A glassy carbon electrode is selected for kinetic measurements because of its high conductivity and controlled electrochemical surface area as compared with traditionally used porous graphite felts, which suffer from large ohmic resistances.[38,39] The glassy carbon disk electrode is polished with a 0.05 $\mu$m alumina slurry followed by sonication in deionized water before each electrochemical measurement (procedure elaborated in section S1). Consistent kinetic parameters from multiple runs confirm the reproducibility of this cleaning process. The reference electrode is a single-junction Ag/AgCl electrode calibrated to the reversible hydrogen electrode (RHE), and the counter electrode is a graphite rod that is separated from the working electrolyte compartment by a Nafion 117 membrane. The electrochemical cell is continuously blanketed with $N_2$ gas during all electrochemical kinetic measurements, which are conducted at room temperature ($T$ = 23.3 °C), unless indicated otherwise.

The intrinsic activities in different electrolytes are measured by two independent methods: (1) steady-state current measurements to estimate exchange current densities using the Tafel equation ($i_{o,Tafel}$) and (2) electrochemical impedance spectroscopy (EIS) to first estimate the $V^{2+}/V^{3+}$ charge transfer resistances ($R_{ct}$) at open-circuit voltage (OCV) and then calculate exchange current densities from $R_{ct}$ ($i_{o,R_{ct}}$) using eq 1, as discussed below. The $i_{o,Tafel}$ values are determined from the $y$-intercept of the log of oxidation current densities ($V^{2+} \rightarrow V^{3+} + e^-$). We use the oxidation rather than the reduction currents for $i_{o,Tafel}$ to avoid the convoluting effect of hydrogen evolution in the reduction currents (Figure S3). We confirm that we are not limited by mass transport by operating at a sufficiently high rotation speed where $i_{o,Tafel}$ is unaltered with further increase in rotation rates (Figure S4).

An example of a Tafel plot for different total vanadium concentrations at 30% SoC in $H_2SO_4$ that we used to extract the $i_{o,Tafel}$ values is shown in Figure 1a. The Tafel plots at other SoCs in $H_2SO_4$ are included in Figures S5 and S6. The OCV and $i_{o,Tafel}$ in $H_2SO_4$ are found to be independent of the total vanadium ion concentration but dependent on the SoC, Figure 1b. The shift in OCV toward a more positive potential with a decrease in the SoC in Figure 1b is expected from the Nernst equation (eq S8) and confirms our SoC measurements by UV−vis. The $i_{o,Tafel}$ values obtained for glassy carbon in $H_2SO_4$ at 50% SoC ($(2.89 \pm 0.01) \times 10^{-3}$ mA cm$^{-2}$) are in close agreement with previously reported values on carbon electrodes in $H_2SO_4$ ($(1.76–2.28) \times 10^{-3}$ mA cm$^{-2}$).[12,40] The Tafel slopes ($b$) in Figure 1c, ranging from 120 to 140 mV decade$^{-1}$, correspond to a rate-determining step (RDS) with one-electron transfer, that is, $n_k$ = 1 (eq S16). The nearly constant Tafel slopes indicate no change in mechanism at different total vanadium ion concentrations and SoCs.

The dependence of the exchange current density on the $V^{2+}$ and $V^{3+}$ concentrations serves as new evidence to support the hypothesis that $V^{2+}/V^{3+}$ is an inner-sphere reaction on carbon. A kinetic model of the form $i_o \propto [V^{2+}]^{\alpha}[V^{3+}]^{-\alpha}$ (eq S7), where $\alpha$ is the (positive) reaction order in $V^{2+}$ and $-\alpha$ is the (negative) reaction order in $V^{3+}$, can be used to describe the observed behavior of $i_o$. This kinetic model captures both the $i_o$ independence of total vanadium ion concentration and the increase with SoC (i.e., greater $V^{2+}$ concentration) shown in Figure 1b. The negative order dependence of $i_o$ in $[V^{3+}]$ indicates an adsorption event in the reaction mechanism.[41] This presence of an adsorption event corroborates previous reports that the $V^{2+}/V^{3+}$ redox reaction is an inner-sphere electron transfer reaction.[29−34] The kinetic model (eq S7) and its derivation are discussed in more detail in section S3.

The $i_o$ (in mA cm$^{-2}$) can also be evaluated using $R_{ct}$ (in Ω cm$^2$)[42] from eq 1 (derived in section S4)

$$i_{o,R_{ct}} = \frac{RT}{n_k F R_{ct} n} \tag{1}$$

where $n_k$ is the number of electrons in the RDS, $n$ is the total number of electrons involved in the overall reaction, $F$ is Faraday's constant, $R$ is the universal gas constant, and $T$ is the temperature in K. From fitting of the EIS data at OCV to determine $R_{ct}$ and assuming $n$ = 1, the $i_{o,R_{ct}}$ values are in close quantitative agreement with the $i_{o,Tafel}$ values in $H_2SO_4$, Figure 1d, confirming the accuracy of the measurements of the exchange current densities by both methods. The $i_{o,R_{ct}}$ and $i_{o,Tafel}$ values have similar magnitudes and show the same variation with SoC at elevated temperatures as well, with a percentage root-mean-square error (RMSE) of ∼24% (Figure S7). The $R_{ct}$ values are included in Table S3, and examples of Nyquist plots used to determine $R_{ct}$ in $H_2SO_4$ at −0.43 V vs RHE and the equivalent circuit are shown in Figure S8.

To probe the impact of anions on the intrinsic $V^{2+}/V^{3+}$ redox kinetics, we conducted rate measurements in $HCl/H_2SO_4$ and HCl on glassy carbon to compare with $H_2SO_4$. The





DOI: 10.1021/acsenergylett.9b01423
ACS Energy Lett. 2019, 4, 2368−2377

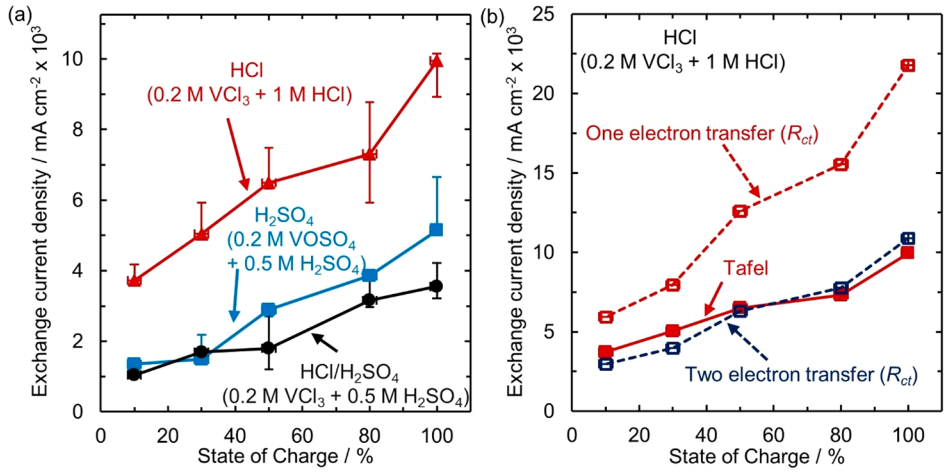


**Figure 2. Exchange current densities as a function of SoC. (a) Evaluated using the Tafel equation in HCl (0.2 M $VCl_3$ + 1 M HCl), $H_2SO_4$ (0.2 M $VOSO_4$ + 0.5 M $H_2SO_4$), and HCl/$H_2SO_4$ (0.2 M $VCl_3$ + 0.5 M $H_2SO_4$). (b) Evaluated in HCl obtained by two independent methods: (i) (solid line) Using the Tafel equation for the reaction $V^{2+} \rightarrow V^{3+} + e^-$ and (ii) (dashed lines) charge transfer resistance at OCV assuming a total of one- and two-electron transfer.**

$i_{o,Tafel}$ in Figure 2a, $b$ (Figure S9), and $i_{o,R_{ct}}$ (Figure S10) are the same in HCl/$H_2SO_4$ as those in $H_2SO_4$, indicating the same reaction mechanism involving one-electron transfer ($n$ = 1). In HCl, however, $i_{o,Tafel}$ is ~2.5 times higher than that in $H_2SO_4$ or HCl/$H_2SO_4$, Figure 2a, but shows the same dependence on SoC. The $i_{o,R_{ct}}$ in HCl is larger than $i_{o,Tafel}$ in HCl when assuming a total of one-electron transfer ($n$ = 1), but if we instead assume that the $V^{2+}$/ $V^{3+}$ overall reaction involves two-electron transfer when converting from $R_{ct}$ to $i_{o,R_{ct}}$ ($n$ = 2) using eq 1, the values of $i_{o,R_{ct}}$ and $i_{o,Tafel}$ in HCl match, as shown in Figure 2b. The $i_{o,R_{ct}}$ and $i_{o,Tafel}$ are also in close agreement in HCl at different temperatures with a percentage RMSE of ~12.5% (Figure S11), only if $n$ = 2. The Tafel slopes in HCl (Figure S9) are similar to those of $H_2SO_4$ and HCl/$H_2SO_4$, both corresponding to a RDS involving one-electron transfer ($n_k$ = 1). Note that this observation is not necessarily inconsistent as the Tafel slope corresponds to the electron transfer in the RDS, whereas the value of $n$ = 2 corresponds to the total number of electrons transferred in the reaction. However, regardless of whether $n$ = 1 or 2, $i_{o,R_{ct}}$ in HCl is larger than the $i_{o,R_{ct}}$ in $H_2SO_4$ and HCl/$H_2SO_4$, confirming the faster kinetics determined from $i_{o,Tafel}$ values shown in Figure 2a. The comparison of $R_{ct}$ in HCl and $H_2SO_4$ at various temperatures is shown in Figure S12, with fitted data from the Nyquist plots included in Tables S3 and S4. Examples of Nyquist plots comparing $R_{ct}$ in $H_2SO_4$ and HCl at −0.43 V vs RHE are shown in Figures S8 and S13.

The various kinetic parameters evaluated in HCl compared to those in HCl/$H_2SO_4$ and $H_2SO_4$ suggest a change in mechanism on glassy carbon in HCl. From the agreement of $i_{o,Tafel}$ and $i_{o,R_{ct}}$ with $n$ = 2 in HCl but with $n$ = 1 in HCl/$H_2SO_4$ and $H_2SO_4$, the total number of electrons transferred appears to change. However, the number of electrons in the RDS remains the same, based on the similar Tafel slopes in all three electrolytes. Because of the dependence of $i_o$ on SoC in all three electrolytes, it is likely that the mechanism proceeds through an inner-sphere adsorbate-mediated step in all three electrolytes; however, the increase in exchange current densities in HCl may be a result of a change in the adsorbed intermediate species.

Further support for a different mechanism in HCl comes from the lower apparent activation energies ($E_a$) in HCl compared to those in $H_2SO_4$ at a given SoC. $E_a$ values evaluated from $i_{o,Tafel}$ (from steady-state rate measurements) and $i_{o,R_{ct}}$ (from EIS) are consistent with one another for a given electrolyte, and both indicate lower activation energies for the $V^{2+}/V^{3+}$ reaction in HCl, as shown in Figure 3. The Arrhenius plots used to derive the apparent activation energies are included in Figure S14, with $E_a$ values in Table S5.

The variation of $E_a$ with SoC also supports our hypothesis of the $V^{2+}/V^{3+}$ reaction being an inner-sphere reaction involving an adsorption event, as opposed to an outer-sphere reaction where $E_a$ is expected to be independent of SoC.[43] The $E_a$ increases with decreasing SoC (Figure 3) in HCl and $H_2SO_4$, which supports our previously discussed observations of

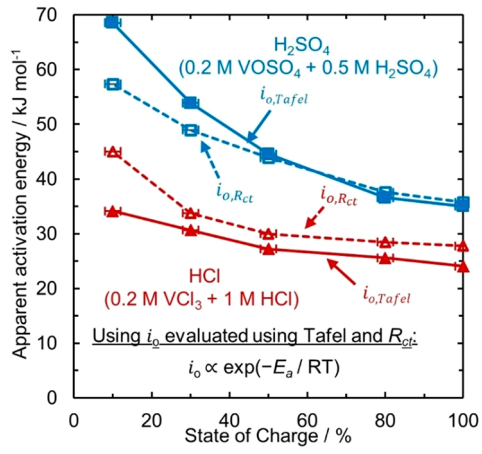


**Figure 3. Apparent activation energies ($E_a$) for the $V^{2+}/V^{3+}$ redox reaction on a glassy carbon working electrode as a function of SoC for $H_2SO_4$ (0.2 M $VOSO_4$ + 0.5 M $H_2SO_4$) and HCl (0.2 M $VCl_3$ + 1 M HCl) from exchange current densities obtained by using (solid lines) the Tafel equation ($i_{o,Tafel}$) and (dashed lines) charge transfer resistance ($i_{o,R_{ct}}$) at OCV. The $i_{o,Tafel}$ and $i_{o,R_{ct}}$ were evaluated at each SoC at $T$ = 23.3, 30.0, 35.0, and 40.0 °C.**



DOI: 10.1021/acsenergylett.9b01423
ACS Energy Lett. 2019, 4, 2368−2377

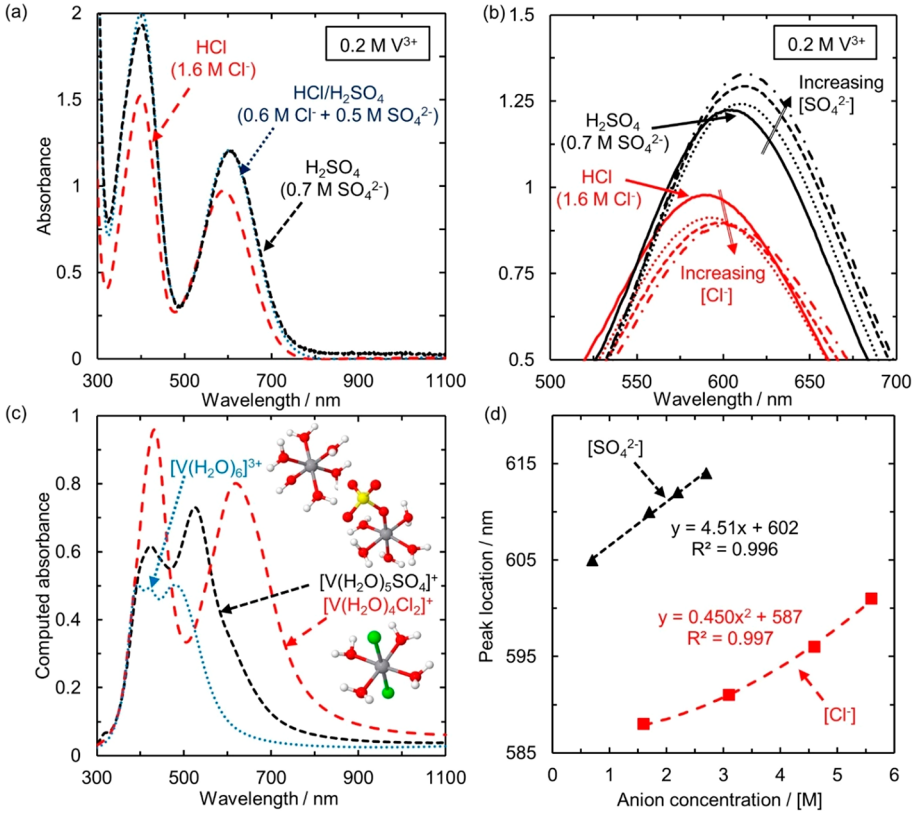


**Figure 4. UV−vis absorbance as a function of wavelength. (a) Experimental $V^{3+}$ spectra for HCl (0.2 M $VCl_3$ + 1 M HCl), $H_2SO_4$ (0.2 M $VOSO_4$ + 0.5 M $H_2SO_4$), and HCl/$H_2SO_4$ (0.2 M $VCl_3$ + 0.5 M $H_2SO_4$) obtained by reducing vanadium salt (either $VOSO_4$ or $VCl_3$) completely to $V^{2+}$ and oxidizing back to $V^{3+}$. (b) $^3T_{1g} \rightarrow {}^3T_{2g}$ transition peak for $V^{3+}$ solutions obtained as in (a) followed by addition of sodium sulfate and sodium chloride separately to obtain spectra at various $SO_4^{2-}$ (0.7, 1.7, 2.2, and 2.7 M $SO_4^{2-}$) and $Cl^-$ (1.6, 3.1, 4.6, and 5.6 M $Cl^-$) concentrations. (c) Theoretical $V^{3+}$ spectra of complexes $[V(H_2O)_6]^{3+}$, $[V(H_2O)_5SO_4]^+$, and $[V(H_2O)_4Cl_2]^+$ obtained by TDDFT. For atom/ions in complex, gray depicts vanadium, red is for oxygen, white is for hydrogen, green is for chloride, and yellow is for sulfur. (d) Experimental peak location of the $^3T_{1g} \rightarrow {}^3T_{2g}$ transition for the $V^{3+}$ complex at various $SO_4^{2-}$ and $Cl^-$ concentrations (as in (b)) showing first-order dependence on $[SO_4^{2-}]$ and second-order dependence on $[Cl^-]$.**

increasing $i_o$ with SoC (Figure 2a). The decrease in the apparent activation energies in HCl corresponds qualitatively to an increase in $i_{o,Tafel}$ and decrease of $R_{ct}$ in HCl compared with that in $H_2SO_4$. However, quantitatively, the ∼2.5 times rate enhancement in HCl is $\sim 10^2$ orders lower than would be expected from the decrease in $E_a$ (∼17 kJ $mol^{-1}$ decrease for 50% SoC evaluated by $i_{o,Tafel}$) in comparison to that in $H_2SO_4$, assuming that the sole difference in rate is from the activation energies (i.e., no change in the pre-exponential factor). To understand whether changes in mechanism in HCl compared with that in $H_2SO_4$ and HCl/$H_2SO_4$ could arise from differences in the vanadium complex structure that can alter the adsorbed intermediate, we examine the structure of $V^{2+}$ and $V^{3+}$ complexes.

We use UV−vis to identify the vanadium complexes formed in bulk solutions of different electrolytes and to probe whether the complex's structure is responsible for the rate enhancement of $V^{2+}/V^{3+}$ in HCl. The UV−vis spectra of $V^{2+}$ and $V^{3+}$ in noninteracting $HClO_4$ are used as a reference for the water-only complexes[28] to enable a comparison to $V^{2+}$ and $V^{3+}$ spectra in the presence of other anions ($Cl^-$ and $SO_4^{2-}$). The UV−vis of $V^{2+}$ shows the same peak intensities and locations in HCl, $H_2SO_4$, HCl/$H_2SO_4$, and $HClO_4$ (Figure S15), indicating that there is no difference in the first coordination sphere of $V^{2+}$ in the four acidic electrolytes. As $H_2O$ is the only common ligand in all four electrolytes of HCl, $H_2SO_4$, HCl/$H_2SO_4$, and $HClO_4$, we conclude that the $[V(H_2O)_6]^{2+}$ proposed in previous studies[27,28] is the dominant $V^{2+}$ species in all electrolytes used in our kinetic studies.

Unlike $V^{2+}$, the UV−vis spectrum of $V^{3+}$ changes with electrolyte, where the peak location of the lower-energy $^3T_{1g} \rightarrow {}^3T_{2g}$ transition[44,45] is at 588 nm in HCl and $HClO_4$ (HCl and $HClO_4$ are compared in Figure S16) and 605 nm in HCl/$H_2SO_4$ and $H_2SO_4$, shown in Figure 4a. The peak corresponding to a higher-energy transition ($^3T_{1g}$ (F) → $^3T_{1g}$ (P)) shifts less than the $^3T_{1g} \rightarrow {}^3T_{2g}$ upon anion complexation in both experimental (Figure 4a) and computational (Figure 4c) $V^{3+}$ UV−vis spectra. The dependence of the peak location on the electrolyte implies that, unlike $V^{2+}$, the $V^{3+}$ coordinates with anions in at least one of the electrolytes, Figure 4a. Figure S17 shows the computationally derived UV−vis spectra of different $V^{3+}$ complexes with their possible orbital transitions. Details of the UV−vis spectra assignments are provided in Table S6.

The peak locations in the $V^{3+}$ spectra in HCl (1.6 M $Cl^-$) appear at ∼400 nm ($^3T_{1g}$ (F) → $^3T_{1g}$ (P))[44,45] and ∼588 nm ($^3T_{1g} \rightarrow {}^3T_{2g}$)[44,45] and resemble the spectra of $[V(H_2O)_6]^{3+}$ with only the perchlorate anion present (Figure S16).[28] As the $Cl^-$ concentration is increased from 1.6 to 5.6 M, the $^3T_{1g} \rightarrow {}^3T_{2g}$ peak shifts to higher wavelengths, Figure 4b, in agreement with previous studies of $V^{3+}$ at high $Cl^-$ concentrations.[28,46] We attribute this shift to an increase in the fraction of $V^{3+}$



DOI: 10.1021/acsenergylett.9b01423
ACS Energy Lett. 2019, 4, 2368−2377

**Scheme 1. Proposed Catalytic Cycle of $V^{2+}$ Oxidation to $V^{3+}$ on Glassy Carbon**[a]

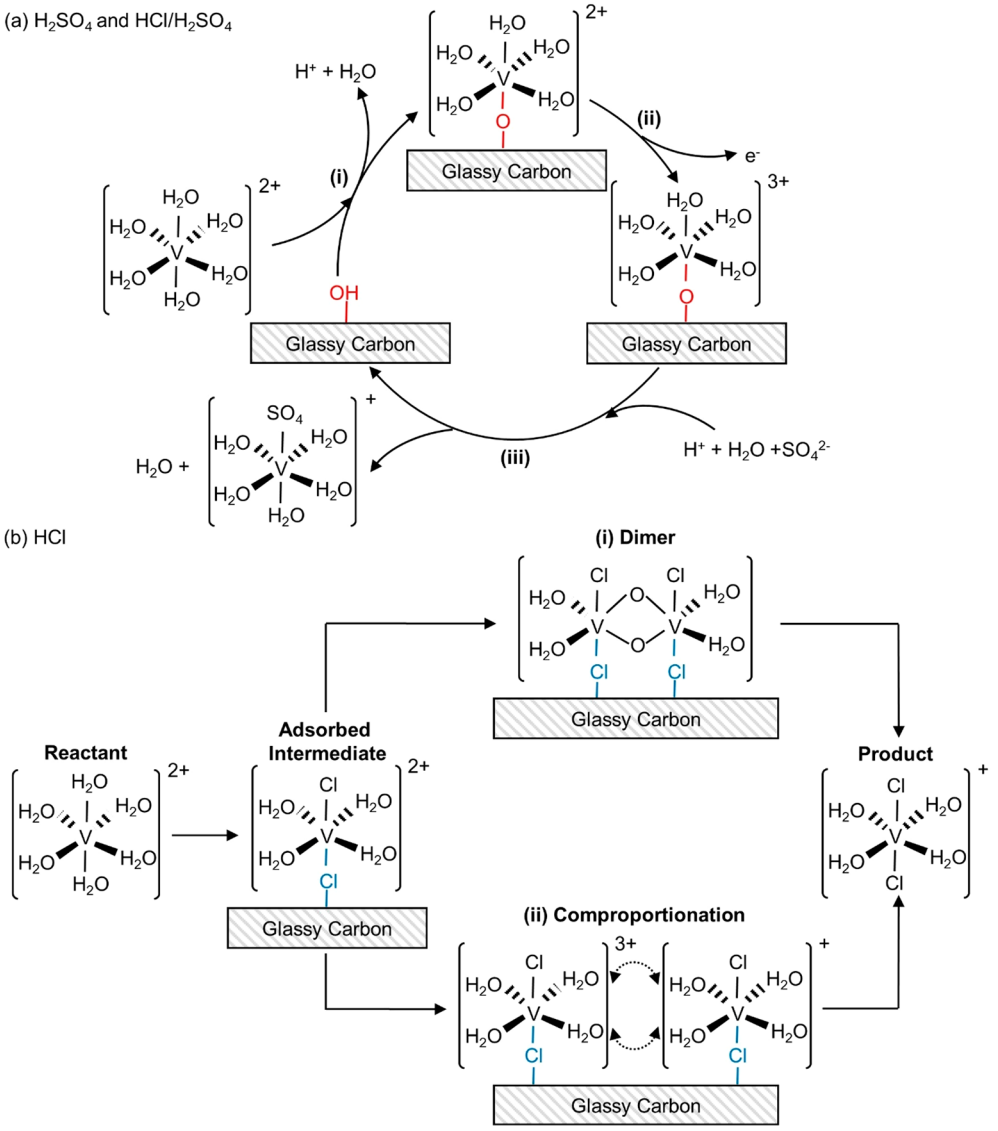


[a](a) In $H_2SO_4$ and $HCl/H_2SO_4$: (i) The $V^{2+}$ ion as $[V(H_2O)_6]^{2+}$ adsorbs to *OH on the glassy carbon surface after shedding a water ligand. The adsorption of $V^{2+}$ involves the loss of a proton, forming $*O[V(H_2O)_5]^{2+}$. (ii) Electron transfer occurs through the *OH, acting as a bridge and leading to oxidation of $V^{2+}$ to $V^{3+}$. We call the bridge here *OH by convention, although it may be an *O bridge due to the loss of the proton to the solution. (iii) The adsorbed intermediate $*O[V(H_2O)_5]^{3+}$ desorbs (taking on a water or sulfate ligand), with addition of $H^+$ leading to regeneration of the adsorbed *OH species on the glassy carbon surface. $[V(H_2O)_6]^{3+}$ in the bulk electrolyte can exchange a water ligand with $SO_4^{2-}$ to form $[V(H_2O)_5SO_4]^+$, or it may directly take the $SO_4^{2-}$ ligand when desorbing. (b) In HCl: $V^{2+}$ adsorbs onto the glassy carbon surface through a *Cl bridge. The adsorbed species may undergo two-electron transfer via two possible postulated routes. (i) Two adsorbed vanadium intermediates can interact to form a dimer, facilitating two-electron transfer, followed by desorption/dissociation to give $[V(H_2O)_4Cl_2]^+$. (ii) Adsorbed $V^{2+}$ can undergo a comproportionation reaction with adsorbed $V^{4+}$ formed as an intermediate to form $V^{3+}$, which desorbs to give product $[V(H_2O)_4Cl_2]^+$. Note that $[V(H_2O)_5SO_4]^+$ shown in (a) is the majority complex formed in $H_2SO_4$ and $HCl/H_2SO_4$, while $[V(H_2O)_4Cl_2]^+$ shown in (b) is the minority complex formed in HCl because we believe that these are the kinetically most relevant species in the given electrolytes, as discussed in the main text. $V^{3+}$reduction is assumed to follow the reverse reaction.

complexes with $Cl^-$ in the $V^{3+}$ coordination sphere rather than only water. Our theoretical UV−vis spectrum for $[V(H_2O)_4Cl_2]^+$ also shows a shift toward higher wavelengths compared to $[V(H_2O)_6]^{3+}$, Figure 4c. Thus, in the HCl electrolyte that we used for kinetic studies (1.6 M $Cl^-$), we have a distribution of $V^{3+}$ complexes with chloride (either of the form $[V(H_2O)_5Cl]^{2+}$ or $[V(H_2O)_4Cl_2]^+$ based on previous DFT studies[24,26]) and water only ($[V(H_2O)_6]^{3+}$), although the exact distribution cannot be determined without knowing the exact peak locations for the pure coordinated complex. The $^3T_{1g} \rightarrow {}^3T_{2g}$ peak location shows a second-order dependence on $[Cl^-]$, as shown in Figure 4d, indicating that $[V(H_2O)_4Cl_2]^+$ forms in HCl rather than $[V(H_2O)_5Cl]^{2+}$ because the single chloride complex cannot show a second-order dependence in $[Cl^-]$. This structural assignment requires the assumption that the peak location is proportional to the ratio of the chloride complex to the total amount of $V^{3+}$, as discussed in section S5.

In $H_2SO_4$, with increasing $SO_4^{2-}$ concentrations, the $^3T_{1g} \rightarrow {}^3T_{2g}$ transition peak shifts toward higher wavelengths



DOI: 10.1021/acsenergylett.9b01423
ACS Energy Lett. 2019, 4, 2368−2377

compared with HCl, Figure 4b, indicating that $SO_4^{2-}$ enters the first coordination sphere of $V^{3+}$. We hypothesize that $[V(H_2O)_6]^{3+}$ undergoes ligand exchange to form $[V(H_2O)_5SO_4]^+$ in $H_2SO_4$ because the $^3T_{1g} \rightarrow {}^3T_{2g}$ peak location shows a first-order dependence on $[SO_4^{2-}]$, Figure 4d, as opposed to the second-order seen for chloride. The argument that $[V(H_2O)_5SO_4]^+$ is formed in $H_2SO_4$ rather than $[V(H_2O)_4(SO_4)_2]^-$ is further supported by the higher absolute absorbance of the $^3T_{1g}$ (F) $\rightarrow {}^3T_{1g}$ (P) and $^3T_{1g} \rightarrow {}^3T_{2g}$ transitions compared with the $[V(H_2O)_6]^{3+}$ complex in both experimental (Figure 4a) and computational (Figure 4c) UV−vis spectra, attributed to the loss of the inversion center and $O_h$ symmetry by addition of a single sulfate ligand in the $V^{3+}$ coordination sphere. The $V^{3+}$ spectrum in $HCl/H_2SO_4$ shows the same peak locations and intensity as $H_2SO_4$, Figure 4a; thus, we infer that a similar complex distribution is present (i.e., $[V(H_2O)_5SO_4]^+$ and $[V(H_2O)_6]^{3+}$) in both of these electrolytes. The absence of the $[V(H_2O)_4Cl_2]^+$ complex in $HCl/H_2SO_4$ (and in other mixtures of $Cl^-/SO_4^{2-}$ shown in Figure S18) as identified by UV−vis is likely due to the stronger complexation of sulfate than chloride. This stronger complexation of sulfate than chloride is supported by our DFT calculations of ligand-exchange free energies (discussed in further detail in section S6).

We assume that at sufficiently low vanadium concentrations the fraction of vanadium ions in dimers is minimal. However, as the vanadium concentration is increased, the formation of dimers becomes thermodynamically more favorable, and the increase in the fraction of dimers in solution would result in the appearance of either new transition peaks or new shoulders in existing transition peaks in the UV−vis spectra.[47] As we do not observe changes in peak shapes or the appearance of new transition peaks in the UV−vis spectra of $V^{2+}$ and $V^{3+}$ (Figure S1) with increasing vanadium concentration, we assume that no vanadium dimers are formed in our tested electrolytes.

Our analysis indicates that the improvement in the kinetics in HCl arises only when the $[V(H_2O)_4Cl_2]^+$ complex is present. The appreciable decrease in apparent activation energies (~17 kJ $mol^{-1}$ lower in HCl at 50% SoC evaluated by $i_{o,Tafel}$), Figure 3, but rather modest increase in rate (~2.5 times) for HCl compared to that for $H_2SO_4$ or the $HCl/H_2SO_4$ mixture, Figure 2a, may be because there is only a small fraction of the more kinetically active $[V(H_2O)_4Cl_2]^+$ complex in HCl, with the balance being the less active $[V(H_2O)_6]^{3+}$. Thus, the pre-exponential factor may be different for the two mechanisms, i.e., lower in HCl, but because the apparent activation energies are lower, the overall kinetics are faster in HCl.

We hypothesize that the higher $V^{2+}/V^{3+}$ activity in HCl arises because the charge transfer occurs through a chloride bridge (*Cl) in HCl, shown in Scheme 1b, as opposed to an OH bridge (*OH) in $H_2SO_4$ (Scheme 1a). Carbon electrodes are occupied with surface hydroxyl (*OH) groups in aqueous media,[36] which have been hypothesized to act as a bridge for electron transfer in $H_2SO_4$ for the $V^{2+}/V^{3+}$ reaction,[35] consistent with the inner-sphere mechanism behavior that we observed here. Chloride is known to adsorb on carbon electrodes,[48] and the *Cl bridge enhances the electron transfer compared with the *OH bridge for metal ions because of the higher polarizability of *Cl compared with that of *OH.[37,49,50] A rate enhancement in the presence of $Cl^-$ has been reported for $Cr^{2+}/Cr^{3+}$,[51,52] $Fe^{2+}/Fe^{3+}$,[53] and $Cu^{2+}/Cu^+$ redox couples[54] on metal electrodes, hypothesized to be due to *Cl acting as a bridge for electron transfer. To our knowledge, the apparent activation energies of a *Cl vs *OH bridge for an inner-sphere reaction over an electrode surface have not been previously reported for $V^{2+}/V^{3+}$ or other similarly behaving redox couples like $Cr^{2+}/Cr^{3+}$, $Fe^{2+}/Fe^{3+}$, and $Cu^{2+}/Cu^+$.

To further test this mechanistic hypothesis involving bridges, we examined the $V^{2+}/V^{3+}$ redox kinetics in HBr, where we postulated a greater kinetic enhancement due to the formation of a highly polarizable *Br bridge compared with a *Cl bridge.[37,50] Indeed, our current density measurements vs overvoltage show a ~1.5 times rate enhancement in HBr ($(9.82 \pm 0.04) \times 10^{-3}$ mA $cm^{-2}$) compared with HCl ($(6.49 \pm 0.09)) \times 10^{-3}$ mA $cm^{-2}$), as shown in Figure S19, and a ~3.5 times rate enhancement compared with $H_2SO_4$ ($(2.89 \pm 0.01) \times 10^{-3}$ mA $cm^{-2}$) at 50% SoC. The dominant $V^{2+}$ and $V^{3+}$ complexes in HBr are the same as those identified in HCl using UV−vis spectroscopy, i.e., a $[V(H_2O)_6]^{2+}$ complex for $V^{2+}$ and a distribution of complexes with the majority as $[V(H_2O)_6]^{3+}$ and minority as $[V(H_2O)_5Br]^{2+}$ or $[V(H_2O)_4Br_2]^+$ for $V^{3+}$ (Figure S20). Rate enhancement in HBr compared with HCl has been reported for the $V^{2+}/V^{3+}$ redox couple on mercury electrodes due to bromide bridging,[55] but there have been no reports for this enhancement observed on carbon electrodes.

Ultimately, there are several pieces of evidence that support the formation of a chloride intermediate for the $V^{2+}/V^{3+}$ reaction. In bulk solution, UV−vis shows the presence of small concentrations of $[V(H_2O)_4Cl_2]^+$ in HCl, which is supported by our DFT calculations. When this complex is observed, the reaction has a lower apparent activation barrier, a higher exchange current density, and a change in the total number of electrons involved, implying a change in mechanism, which we attribute to the involvement of the chloride species in the reaction. Previous kinetic studies of other redox couples like $Cr^{2+}/Cr^{3+}$,[51,52] $Fe^{2+}/Fe^{3+}$,[53] and $Cu^{2+}/Cu^+$ in the presence of chloride[54] showed enhanced kinetics in comparison with noninteracting $HClO_4$, which were attributed to *Cl acting as a bridge instead of *OH. The faster electron transfer kinetics of the *Cl compared to the *OH were predicted to be due to better electronic coupling based on ab initio molecular orbital theory calculations.[54] The improved kinetics for the $V^{2+}/V^{3+}$ reaction that we observe in HBr in comparison with HCl also imply that the halide is part of a reaction intermediate. However, the chloride (or bromide) surface intermediate has not been detected in any of the systems mentioned above. In situ or operando spectroscopy techniques such as X-ray absorption, nuclear magnetic resonance, and Raman are necessary to identify the structure of the adsorbed intermediate and will be the focus of future work. Computational studies using techniques such as ab initio metadynamics to compute adsorption and reaction free energies[24,36,56] could also help clarify the possibility of a chloride intermediate on the electrode surface.

As summarized in Scheme 1a, in $H_2SO_4$ and $HCl/H_2SO_4$, we propose that the hexa-aqua $V^{2+}$ complex, $[V(H_2O)_6]^{2+}$, binds with the adsorbed *OH after shedding a water ligand, similar to trivalent chromium.[57] The $V^{2+}$ adsorption process involves loss of a proton, forming an $*O[V(H_2O)_5]^{2+}$ intermediate (i.e., $V^{2+}$ adsorbed to glassy carbon via an *OH bridge). This intermediate then transfers an electron through the *OH bridge to oxidize $V^{2+}$ to $V^{3+}$. After the electron transfer, the $*O[V(H_2O)_5]^{3+}$ intermediate desorbs, taking a water or sulfate ligand into the bulk electrolyte. In the bulk





DOI: 10.1021/acsenergylett.9b01423
ACS Energy Lett. 2019, 4, 2368−2377

solution, $[V(H_2O)_6]^{3+}$ can undergo ligand exchange to replace the $H_2O$ ligand by $SO_4^{2-}$, or $SO_4^{2-}$ can be added directly during the desorption step, forming the $[V(H_2O)_5SO_4]^+$ seen by UV−vis in $H_2SO_4$ and $HCl/H_2SO_4$. We attribute the similar kinetics that we observe in $HCl/H_2SO_4$ and $H_2SO_4$ to the high $SO_4^{2-}$ concentration in $HCl/H_2SO_4$, which causes $[V(H_2O)_5SO_4]^+$ to dominate as opposed to $[V(H_2O)_4Cl_2]^+$. We hypothesize that at sufficiently high $Cl^-$ concentrations, even in mixed $HCl/H_2SO_4$ systems, there may be a catalytic effect such as that observed in HCl, possibly explaining the higher current densities in mixed-acid full cell systems,[19−21] where the $Cl^-$ concentrations are much higher than those used in our work here. Future work on the concentration dependence is needed to verify this hypothesis.

In HCl, the adsorbed $Cl^-$ (*Cl) on glassy carbon can act as a bridge for electron transfer (Scheme 1b). On the basis of the results from impedance and steady-state current measurements, this mechanism is an overall two-electron transfer with a one-electron RDS. Although we do not have definitive proof for a specific mechanism, we propose two mechanisms here that are consistent with our measured data. One possible mechanism is that two adsorbed vanadium intermediates form a dimer on the carbon surface to facilitate two-electron transfer, after which the dimer desorbs/dissociates (no dimers were detected in bulk solution by UV−vis, as mentioned above). Another possible mechanism involves formation of $V^{4+}$ as a reaction intermediate, which reacts with $V^{2+}$, undergoing a comproportionation reaction observed in a previous study in perchlorate solutions[58] to give $V^{3+}$, facilitating an overall two-electron transfer. A similar mechanism as that shown in Scheme 1b may occur in HBr, but additional tests are needed and will be the focus of future work.

In summary, this work gives further evidence that the $V^{2+}/V^{3+}$ reaction involves inner-sphere electron transfer on glassy carbon, based on rate measurements in different electrolytes that confirm the presence of an adsorbed intermediate. The precise inner-sphere mechanism is shown to depend on the choice of acidic electrolyte, based on different rates, activation energies, and the total number of electrons transferred. Two independent electrochemical techniques for estimating $i_o$ indicate faster $V^{2+}/V^{3+}$ redox kinetics with an overall two-electron transfer in HCl as opposed to a kinetically slower single-electron transfer in $H_2SO_4$ and $HCl/H_2SO_4$. UV−vis spectroscopy measurements confirm that $V^{2+}$ is complexed by water only as $[V(H_2O)_6]^{2+}$ and identify the $V^{3+}$ complexes formed in the electrolytes in which we measured $V^{2+}/V^{3+}$ kinetics. In HCl, the $V^{3+}$ exists as a mixture of $[V(H_2O)_6]^{3+}$ and $[V(H_2O)_4Cl_2]^+$, whereas in $H_2SO_4$ and $HCl/H_2SO_4$, the $V^{3+}$ exists as a mixture of $[V(H_2O)_5SO_4]^+$ and $[V(H_2O)_6]^{3+}$. We hypothesize that the electron transfer in the $V^{2+}/V^{3+}$ reaction goes through a bridging ligand, and the higher rate in HCl than that in $H_2SO_4$ or $HCl/H_2SO_4$ is due to the higher polarizability of the *Cl bridge than the *OH bridge, which leads to enhanced electron transfer through the *Cl bridge. This is supported by testing the $V^{2+}/V^{3+}$ redox kinetics in HBr, which shows higher activity than that in HCl, attributed to the higher polarizability of *Br compared with *Cl. Electrolyte engineering to ensure the presence of more effective bridges to facilitate electron transfer may be a method to improve VRFB kinetic performance in full cell systems. Overall, this study highlights the importance of identifying the structures of complexed species in interpreting kinetics and the use of multiple independent electrochemical techniques to gain valuable mechanistic insights into fundamental charge transfer reactions.

## ■ ASSOCIATED CONTENT

### Supporting Information

The Supporting Information is available free of charge on the ACS Publications website at DOI: 10.1021/acsenergylett.9b01423.

Experimental procedures (electrolyte preparation, electrochemical cell assembly, electrolysis to control SoC, UV−vis measurements, Gaussian curve fitting, and electrochemical measurements); theoretical UV−vis spectra computed using TDDFT; rate law for $V^{2+}/V^{3+}$ reaction; electrochemical kinetics theory; predicting the number of anions in the $V^{3+}$ inner coordination sphere; stability of $V^{3+}$ complexes by UV−vis spectroscopy and DFT; effect of $H_2$ evolution on experimental OCVs; Tafel plots; Nyquist plots; exchange current densities; charge transfer resistances; Arrhenius plots; UV−vis spectra; calibration parameters; fitted parameters; activation energies; TDDFT transitions; computed free energies; nomenclature; and supporting references (PDF)

## ■ AUTHOR INFORMATION


### Corresponding Author

*E-mail: snirala@umich.edu.

### ORCID

Harsh Agarwal: 0000-0002-5237-4819
Jacob Florian: 0000-0003-1895-8463
Bryan R. Goldsmith: 0000-0003-1264-8018
Nirala Singh: 0000-0003-0389-3927


### Author Contributions

N.S. conceived the project. H.A. carried out all electrochemical measurements and data analysis under the guidance of N.S. J.F. performed all the molecular simulations and DFT modeling under the guidance of B.R.G. All authors were involved in analysis and writing the manuscript.

### Notes

The authors declare no competing financial interest.

## ■ ACKNOWLEDGMENTS

This work was supported by University of Michigan start-up funds of N.S. and B.R.G. We thank Vincent L. Pecoraro and Niri Govind for insightful discussions. We thank Suljo Linic for use of his UV−vis instrument. This research used resources of the National Energy Research Scientific Computing Center (NERSC), a U.S. Department of Energy Office of Science User Facility operated under Contract No. DE-AC02-05CH11231.

## ■ REFERENCES


(1) *International Energy Outlook 2017*; DOE/EIA-0484; U.S. Energy Information Administration, 2017.

(2) Nguyen, T.; Savinell, R. F. Flow Batteries. *Electrochem. Soc. Interface* **2010**, *19*, 54−56.

(3) Dunn, B.; Kamath, H.; Tarascon, J. Electrical Energy Storage for the Grid: A Battery of Choices. *Science* **2011**, *334*, 928−935.

(4) Thaller, L. H. Electrically Rechargeable Redox Flow Cells. *Intersociety Energy Conversion Engineering Conference, 9th, Proceedings* (A75-10476 01-44), San Francisco, CA, Aug 26−30, 1974; pp 924−928.






DOI: 10.1021/acsenergylett.9b01423
*ACS Energy Lett.* 2019, 4, 2368−2377

(5) Gong, K.; Xu, F.; Grunewald, J. B.; Ma, X.; Zhao, Y.; Gu, S.; Yan, Y. All-Soluble All-Iron Aqueous Redox-Flow Battery. *ACS Energy Lett.* **2016**, *1*, 89−93.
(6) Wei, X.; Duan, W.; Huang, J.; Zhang, L.; Li, B.; Reed, D.; Xu, W.; Sprenkle, V.; Wang, W. A High-Current, Stable Nonaqueous Organic Redox Flow Battery. *ACS Energy Lett.* **2016**, *1*, 705−711.
(7) Yu, J.; Fan, L.; Yan, R.; Zhou, M.; Wang, Q. Redox Targeting-Based Aqueous Redox Flow Lithium Battery. *ACS Energy Lett.* **2018**, *3*, 2314−2320.
(8) Skyllas-Kazacos, M.; Rychcik, M.; Robins, R. G.; Fane, A. G.; Green, M. A. New All-Vanadium Redox Flow Cell. *J. Electrochem. Soc.* **1986**, *133*, 1057−1058.
(9) Flow Batteries: Investment and Innovation Trends, Top Deals and Deal-Makers | i3 Connect. https://i3connect.com/tag/flow-batteries (Accessed Jun 5, 2019).
(10) Vanadium Redox Flow Battery (VRFB) Technology is Increasingly being Tested and Deployed Across the Globe. https://willigan.digital/pr/bold-editorial/vanitec/v3/ (Accessed Jun 4, 2019).
(11) Kim, K. J.; Park, M.-S.; Kim, Y.-J.; Kim, J. H.; Dou, S. X.; Skyllas-Kazacos, M. A Technology Review of Electrodes and Reaction Mechanisms in Vanadium Redox Flow Batteries. *J. Mater. Chem. A* **2015**, *3*, 16913−16933.
(12) Aaron, D.; Sun, C.-N.; Bright, M.; Papandrew, A. B.; Mench, M. M.; Zawodzinski, T. A. In Situ Kinetics Studies in All-Vanadium Redox Flow Batteries. *ECS Electrochem. Lett.* **2013**, *2*, A29−A31.
(13) Bourke, A.; Miller, M. A.; Lynch, R. P.; Gao, X.; Landon, J.; Wainright, J. S.; Savinell, R. F.; Buckley, D. N. Electrode Kinetics of Vanadium Flow Batteries: Contrasting Responses of $V^{II}$ -$V^{III}$ and $V^{IV}$ -$V^{V}$ to Electrochemical Pretreatment of Carbon. *J. Electrochem. Soc.* **2016**, *163*, A5097−A5105.
(14) Roznyatovskaya, N.; Noack, J.; Mild, H.; Fühl, M.; Fischer, P.; Pinkwart, K.; Tübke, J.; Skyllas-Kazacos, M.; et al. Vanadium Electrolyte for All-Vanadium Redox-Flow Batteries: The Effect of the Counter Ion. *Batteries* **2019**, *5*, 13.
(15) Skyllas-Kazacos, M. Performance Improvements and Cost Considerations of the Vanadium Redox Flow Battery. *ECS Trans.* **2019**, *89*, 29−45.
(16) Kim, S.; Vijayakumar, M.; Wang, W.; Zhang, J.; Chen, B.; Nie, Z.; Chen, F.; Hu, J.; Li, L.; Yang, Z. Chloride Supporting Electrolytes for All-Vanadium Redox Flow Batteries. *Phys. Chem. Chem. Phys.* **2011**, *13*, 18186−18193.
(17) Skyllas-Kazacos, M. Novel Vanadium Chloride/Polyhalide Redox Flow Battery. *J. Power Sources* **2003**, *124*, 299−302.
(18) Wang, W.; Kim, S.; Chen, B.; Nie, Z.; Zhang, J.; Xia, G.-G.; Li, L.; Yang, Z. A New Redox Flow Battery Using Fe/V Redox Couples in Chloride Supporting Electrolyte. *Energy Environ. Sci.* **2011**, *4*, 4068−4073.
(19) Wang, W.; Nie, Z.; Chen, B.; Chen, F.; Luo, Q.; Wei, X.; Xia, G. G.; Skyllas-Kazacos, M.; Li, L.; Yang, Z. A New Fe/V Redox Flow Battery Using a Sulfuric/Chloric Mixed-Acid Supporting Electrolyte. *Adv. Energy Mater.* **2012**, *2*, 487−493.
(20) Li, L.; Kim, S.; Wang, W.; Vijayakumar, M.; Nie, Z.; Chen, B.; Zhang, J.; Xia, G.; Hu, J.; Graff, G.; et al. A Stable Vanadium Redox-Flow Battery with High Energy Density for Large-Scale Energy Storage. *Adv. Energy Mater.* **2011**, *1*, 394−400.
(21) Vijayakumar, M.; Wang, W.; Nie, Z.; Sprenkle, V.; Hu, J. Elucidating the Higher Stability of Vanadium(V) Cations in Mixed Acid Based Redox Flow Battery Electrolytes. *J. Power Sources* **2013**, *241*, 173−177.
(22) Richens, D. T. Group 5 Elements: Vanadium, Niobium and Tantalum. *The Chemistry of Aqua Ions: Synthesis, Structure and Reactivity*; John Wiley & Sons, Ltd.: Chichester, U.K., 1997; pp 230−235.
(23) Sepehr, F.; Paddison, S. J. The Solvation Structure and Thermodynamics of Aqueous Vanadium Cations. *Chem. Phys. Lett.* **2013**, *585*, 53−58.
(24) Bon, M.; Laino, T.; Curioni, A.; Parrinello, M. Characterization of Vanadium Species in Mixed Chloride−Sulfate Solutions: An Ab Initio Metadynamics Study. *J. Phys. Chem. C* **2016**, *120*, 10791−10798.
(25) Vijayakumar, M.; Li, L.; Nie, Z.; Yang, Z.; Hu, J. Structure and Stability of Hexa-Aqua V(III) Cations in Vanadium Redox Flow Battery Electrolytes. *Phys. Chem. Chem. Phys.* **2012**, *14*, 10233−10242.
(26) Gupta, S.; Lim, T. M.; Mushrif, S. H. Insights into the Solvation of Vanadium Ions in the Vanadium Redox Flow Battery Electrolyte Using Molecular Dynamics and Metadynamics. *Electrochim. Acta* **2018**, *270*, 471−479.
(27) Oldenburg, F. J.; Bon, M.; Perego, D.; Polino, D.; Laino, T.; Gubler, L.; Schmidt, T. J. Revealing the Role of Phosphoric Acid in All-Vanadium Redox Flow Batteries with DFT Calculations and In Situ Analysis. *Phys. Chem. Chem. Phys.* **2018**, *20*, 23664−23673.
(28) Martin, E. L.; Bentley, K. E. Spectrophotometric Investigation of Vanadium(II), Vanadium(III), and Vanadium(IV) in Various Media. *Anal. Chem.* **1962**, *34*, 354−358.
(29) Li, B.; Gu, M.; Nie, Z.; Shao, Y.; Luo, Q.; Wei, X.; Li, X.; Xiao, J.; Wang, C.; Sprenkle, V.; et al. Bismuth Nanoparticle Decorating Graphite Felt as a High-Performance Electrode for an All-Vanadium Redox Flow Battery. *Nano Lett.* **2013**, *13*, 1330−1335.
(30) Yang, X.; Liu, T.; Xu, C.; Zhang, H.; Li, X.; Zhang, H. The Catalytic Effect of Bismuth for $VO_2^+/VO^{2+}$ and $V^{3+}/V^{2+}$ Redox Couples in Vanadium Flow Batteries. *J. Energy Chem.* **2017**, *26*, 1−7.
(31) Wei, L.; Zhao, T. S.; Zeng, L.; Zhou, X. L.; Zeng, Y. K. Copper Nanoparticle-Deposited Graphite Felt Electrodes for All Vanadium Redox Flow Batteries. *Appl. Energy* **2016**, *180*, 386−391.
(32) Mehboob, S.; Mehmood, A.; Lee, J.-Y.; Shin, H.-J.; Hwang, J.; Abbas, S.; Ha, H. Y. Excellent Electrocatalytic Effects of Tin Through In Situ Electrodeposition on the Performance of All-Vanadium Redox Flow Batteries. *J. Mater. Chem. A* **2017**, *5*, 17388−17400.
(33) Shen, J.; Liu, S.; He, Z.; Shi, L. Influence of Antimony Ions in Negative Electrolyte on the Electrochemical Performance of Vanadium Redox Flow Batteries. *Electrochim. Acta* **2015**, *151*, 297−305.
(34) Di Blasi, A.; Busacca, C.; Di Blasi, O.; Briguglio, N.; Antonucci, V. Synthesis and Characterization of Electrospun Nickel-Carbon Nanofibers as Electrodes for Vanadium Redox Flow Battery. *J. Electrochem. Soc.* **2018**, *165*, A1478−A1485.
(35) Sun, B.; Skyllas-Kazacos, M. Chemical Modification of Graphite Electrode Materials for Vanadium Redox Flow Battery Application—Part II. Acid Treatments. *Electrochim. Acta* **1992**, *37*, 2459−2465.
(36) Jiang, Z.; Klyukin, K.; Alexandrov, V. First-Principles Study of Adsorption−Desorption Kinetics of Aqueous $V^{2+}$ /$V^{3+}$ Redox Species on Graphite in a Vanadium Redox Flow Battery. *Phys. Chem. Chem. Phys.* **2017**, *19*, 14897−14901.
(37) Anbar, M.; Hart, E. J. The Reactivity of Metal Ions and Some Oxy Anions toward Hydrated Electrons. *J. Phys. Chem.* **1965**, *69*, 973−977.
(38) Liu, Q. H.; Grim, G. M.; Papandrew, A. B.; Turhan, A.; Zawodzinski, T. A.; Mench, M. M. High Performance Vanadium Redox Flow Batteries with Optimized Electrode Configuration and Membrane Selection. *J. Electrochem. Soc.* **2012**, *159*, A1246−A1252.
(39) Darling, R. M.; Perry, M. L. The Influence of Electrode and Channel Configurations on Flow Battery Performance. *J. Electrochem. Soc.* **2014**, *161*, A1381−A1387.
(40) Fabjan, C.; Garche, J.; Harrer, B.; Jö Rissen, L.; Kolbeck, C.; Philippi, F.; Tomazic, G.; Wagner, F. The Vanadium Redox-Battery: An Efficient Storage Unit for Photovoltaic Systems. *Electrochim. Acta* **2001**, *47*, 825−831.
(41) Xiong, X. Y.; Poorten, H. Vander; Crappe, M. Impedance Parameters of Ni/Cd Batteries-Individual Electrode Characteristics. Application to Modelling and State of Charge Determinations. *Electrochim. Acta* **1996**, *41*, 1267−1275.
(42) Bard, A. J.; Faulkner, L. R. *Electrochemical Methods: Fundamentals and Applications*; John Wiley & Sons, Inc.: New York, 2001.
(43) Weaver, M. J. Activation Parameters for Simple Electrode Reactions. Application to the Elucidation of Ion-Solvent Interactions




DOI: 10.1021/acsenergylett.9b01423
*ACS Energy Lett.* 2019, 4, 2368−2377

in the Transition State for Heterogeneous Electron Transfer. *J. Phys. Chem.* **1979**, *83*, 1748−1757.
(44) Landry-Hum, J.; Bussière, G.; Daniel, C.; Reber, C. Triplet Electronic States in $d^2$ and $d^8$ Complexes Probed by Absorption Spectroscopy: A CASSCF/CASPT2 Analysis of $[V(H_2O)_6]^{3+}$ and $[Ni(H_2O)_6]^{2+}$. *Inorg. Chem.* **2001**, *40*, 2595−2601.
(45) Bussière, G.; Beaulac, R.; Cardinal-David, B.; Reber, C. Coupled Electronic States in Trans-$MCl_2(H_2O)_4^{n+}$ Complexes (M: $Ni^{2+}$, $Co^{2+}$, $V^{3+}$, $Cr^{3+}$) Probed by Absorption and Luminescence Spectroscopy. *Coord. Chem. Rev.* **2001**, *219*−*221*, 509−543.
(46) Furman, S.; Garner, C. Absorption Spectra of Vanadium(III) and Vanadium(IV) Ions in Complexing and Non-Complexing Media. *J. Am. Chem. Soc.* **1950**, *72*, 1785−1789.
(47) Pajdowski, L. A Spectrophotometric Study of the Hydrolysis of Vanadium (III) Ion. *J. Inorg. Nucl. Chem.* **1966**, *28*, 433−442.
(48) Tanimoto, S.; Ichimura, A. Discrimination of Inner and Outer Sphere Electrode Reactions by Cyclic Voltammetry Experiments. *J. Chem. Educ.* **2013**, *90*, 778−781.
(49) Heyrovsky, J. Retarded Electrodeposition of Metals Studies Oscillographically with Mercury Capillary Electrodes. *Discuss. Faraday Soc.* **1947**, *1*, 212−225.
(50) Sykes, A. G. Further Advances in the Study of Mechnaisms of Redox Reactions. *Adv. Inorg. Chem. Radiochem.* **1968**, *10*, 153−245.
(51) Aikens, D. A.; Ross, J. W. Effect of Chloride on the Kinetics of Electroxidation of Chromium (II) in Acidic Perchlorate Medium. *J. Phys. Chem.* **1961**, *65*, 1213−1216.
(52) Rodes, A.; Feliu, J. M.; Aldaz, A.; Clavilier, J. The Influence of Polyoriented Gold Electrodes Modified by Reversibly and Irreversibly Adsorbed Ad-Atoms on the Redox Behaviour of the Cr(III)/Cr(II) Couple and the Effect of Chloride Ions. *J. Electroanal. Chem. Interfacial Electrochem.* **1989**, *271*, 127−139.
(53) Weber, J.; Samec, Z.; Mareček, V. The Effect of Anion Adsorption on the Kinetics of the $Fe^{3+}/Fe^{2+}$ Reaction on Pt and Au Electrodes in $HClO_4$. *J. Electroanal. Chem. Interfacial Electrochem.* **1978**, *89*, 271−288.
(54) Nagy, Z.; Blaudeau, J. P.; Hung, N. C.; Curtiss, L. A.; Zurawski, D. J. Chloride Ion Catalysis of the Copper Deposition Reaction. *J. Electrochem. Soc.* **1995**, *142*, L87−L89.
(55) Niki, K.; Mizota, H. Effect of Specific Adsorbed Anions on the Electrode Kinetics of the V(III)/V(II) and Eu(III)/Eu(II) Couples. *J. Electroanal. Chem. Interfacial Electrochem.* **1976**, *72*, 307−317.
(56) Jiang, Z.; Klyukin, K.; Miller, K.; Alexandrov, V. Mechanistic Theoretical Investigation of Self-Discharge Reactions in a Vanadium Redox Flow Battery. *J. Phys. Chem. B* **2019**, *123*, 3976−3983.
(57) Zeng, Z.; Sun, Y.; Zhang, J. The Electrochemical Reduction Mechanism of Trivalent Chromium in the Presence of Formic Acid. *Electrochem. Commun.* **2009**, *11*, 331−334.
(58) Newton, T. W.; Baker, F. B. The Intermediate in the Reaction between Vanadium(II) and Vanadium(IV). *Inorg. Chem.* **1964**, *3*, 569−573.





DOI: 10.1021/acsenergylett.9b01423
*ACS Energy Lett.* 2019, 4, 2368−2377